UNIVERSITY OF LEEDS

This is a repository copy of *Variations in surface functional groups, carbon chemical state and graphitization degree during thermal deactivation of diesel soot particles*.

White Rose Research Online URL for this paper:
https://eprints.whiterose.ac.uk/182605/

Version: Accepted Version

Article:

Liu, Y orcid.org/0000-0002-9367-3532, Wu, S, Fan, C et al. (3 more authors) (2023) Variations in surface functional groups, carbon chemical state and graphitization degree during thermal deactivation of diesel soot particles. Journal of Environmental Sciences, 124. pp. 678-687. ISSN 1001-0742

https://doi.org/10.1016/j.jes.2022.01.007

© 2022 The Research Center for Eco-Environmental Sciences, Chinese Academy of Sciences. Published by Elsevier B.V. This manuscript version is made available under the CC-BY-NC-ND 4.0 license http://creativecommons.org/licenses/by-nc-nd/4.0/.

Reuse
This article is distributed under the terms of the Creative Commons Attribution-NonCommercial-NoDerivs (CC BY-NC-ND) licence. This licence only allows you to download this work and share it with others as long as you credit the authors, but you can’t change the article in any way or use it commercially. More information and the full terms of the licence here: https://creativecommons.org/licenses/

Takedown
If you consider content in White Rose Research Online to be in breach of UK law, please notify us by emailing eprints@whiterose.ac.uk including the URL of the record and the reason for the withdrawal request.

White Rose
university consortium
Universities of Leeds, Sheffield & York

eprints@whiterose.ac.uk
https://eprints.whiterose.ac.uk/

Variations in surface functional groups, carbon chemical state and graphitization degree during thermal deactivation of diesel soot particles

Ye Liu[a*], Sijin Wu[a], Chenyang Fan[b*], Xin Wang[b], Fangjie Liu[b], Haibo Chen[a]

[a] Institute for Transport Studies, University of Leeds, Leeds LS2 9JT, UK

[b] Vehicle & Transportation Engineering Institute, Henan University of Science and Technology, Luoyang 471003, China

Abstract: The thermal deactivation of diesel soot particles exerts a significant influence on the control strategy for the regeneration of diesel particulate filters (DPFs). This work focused on the changes in the surface functional groups, carbon chemical state, and graphitization degree during thermal treatment in an inert gas environment at intermediate temperatures of 600 °C, 800 °C, and 1000 °C and probes the reason for thermal deactivation. The surface functional groups and carbon chemical state were characterized using Fourier transform infrared spectroscopy (FT-IR) and X-ray photoelectron spectroscopy (XPS). The graphitization degree was evaluated by means of Raman spectroscopy (RS). The concentrations of aliphatic C–H, C–OH, C=O, and O–C=O groups are reduced for diesel soot and carbon black when increasing the thermal treatment temperature, while the sp^2/sp^3 hybridized ratio and graphitization degree enhance. These results provide comprehensive evidence of the decreased reactivity of soot samples. Among oxygenated functional groups, the percentage reduction during thermal treatment is the largest for the O–C=O groups owing to its worst thermodynamic stability.

Keywords: Diesel soot particles; Surface functional groups; Carbon chemical state; graphitization degree; Thermal deactivation

1. Introduction

Currently, diesel particulate filters (DPFs), as a common technology, are widely employed to reduce soot particle emissions and improve air quality (Schejbal et al., 2009). In DPFs, soot particles are trapped until these soot particles will be oxidized when DPF regeneration takes place. The high-temperature exhaust gases varying from 250 to 850 ℃ during this process pass continuously through DPFs (Roth et al., 1998; Matsumoto et al., 2008; Raj et al., 2014). These trapped soot particles undergo thermal treatment for a long time in DPFs, which inevitably causes the thermal deactivation of diesel soot particles. Thermal deactivation means a reduction in reactivity upon thermal treatment (Vander Wal et al., 2004; Sheng, 2007), making diesel soot particles more resistant to be removed when the DPFs regenerate. Thus, it is necessary to probe the reason behind the thermal deactivation to further optimize the control strategy for the DPF regeneration.

Many studies have been conducted concerning the thermal deactivation of carbonaceous materials such as coal char, carbon black, and soot particles (Feng et al., 2002; Sheng, 2007; Raj et al., 2014; Jaramillo et al., 2015). For instance, Feng et al., (2002) studied the impact of thermal treatment in the 850 ℃–1150 ℃ range on the structure and reactivity of the coal char. The results indicated that the thermal deactivation was strongly dependent on the crystallite-perfecting process during thermal treatment. The same conclusions were reached by Sheng (2007), who reported that the increased structural ordering of char crystalline during thermal treatment between 1200 ℃ and 1500 ℃ was responsible for the thermal deactivation. Gaddam et al., (2016) studied the variation in the nanostructure and reactivity of the model carbons when heated to a temperature up to 3000 ℃ under a He atmosphere. The crystallite growth and increase in density during thermal treatment were observed, which caused the decreased reactivity. Jaramillo et al., (2015) explored the changes in nanostructure and reactivity of three model carbons during oxidation at temperatures in the range of 575 °C –775 °C in air. The results presented a good relationship between oxidative reactivity and carbon nanostructure. Zolin et al., (2002) analysed the influence of thermal treatment in an oxygen environment on oxidative reactivity of coal char and found that the elimination of hydrogen and oxygen in the carbonaceous matrix and loss of edge active sites during thermal treatment would lead to a reduction in the oxidative reactivity. However, limited information regarding the changes in the surface functional groups, carbon chemical state, and graphitization degree of diesel soot particles during thermal deactivation is available in a nitrogen environment at temperatures ranging from 600 °C to 1000 °C. Although the exhaust gases passing through a DPF include several gas components, the nitrogen is approximately 70 % or even more in these gases Reşitoğlu et al., (2014). Moreover, the thermal treatment performed under only nitrogen conditions would eliminate the effect of other gas components on the experimental results.

Surface functional groups bonded to non-six-membered carbon rings during the soot oxidation process exert a crucial influence on soot structure and reactivity (Santamaria et al., 2006; Vander Wal et al., 2007). The thermal decomposition of these functional groups would chemically and physically weaken the barriers to lamella reorganization, favouring the rearrangement of carbon lamella and changing the nanostructure (Vander Wal et al., 2007). Simultaneously, the preferential loss of surface functional groups can enhance reactive sites, thereby increasing the soot reactivity (Agudelo et al., 2014; Soriano et al., 2017; Xu et al., 2019). The sp^2 and sp^3 hybridized carbon atoms are primarily chemical states in soot, and the relative amount and spatial relationships are closely associated with the soot structure and reactivity (Vander Wal et al., 2016). In addition, the degree of graphitization is a vital indicator of soot structural order, which is strongly associated with the in-plane crystallite size, affecting soot reactivity (Sheng, 2007; Liu et al., 2017; Zhou et al., 2022).

In this context, the purpose of the present work is to study the alterations in surface functional groups, carbon chemical state and graphitization degree during thermal treatment of soot samples in an inert gas atmosphere at temperatures ranging from 600 to 1000 ℃ and further explore the reason for thermal deactivation. The carbon chemical state and surface functional groups were characterized by means of X-ray photoelectron spectroscopy (XPS) and Fourier transform infrared spectroscopy (FT-IR). The graphitization degree of soot particles was evaluated using Raman spectroscopy (RS).

2. Experimental setup

2.1. Soot samples

Diesel soot particles were sampled on Teflon filters (R2PL047, PALL, USA) from a four-cylinder, four-stroke and turbo-charged compression ignition diesel engine. Table 1 lists the details of the engine used. The engine operating load and speed were set at 55% of the full load and 1800 rpm. The soot samples were scraped from the filters after sampling for further thermal treatment. Additionally, the Printex-U, a commercial carbon black from Evonik-Degussa, was also examined to compare the properties of the diesel soot and Printex-U because the Printex-U is frequently employed as a surrogate for diesel soot (Vander Wal et al., 2007; Raj et al., 2013).

Table 1. Detailed specifications of the diesel engine

Engine parameters	
Number of cylinders, configuration	Four, in-line
Bore×stroke (mm)	102×108
Compression ratio	17:1
Engine displacement (L)	3.856
Rated power	100 kW@2800 rpm
Maximum torque (N·m)	420
Fuel injection type	Common rail system

2.2. Thermal treatment

For each thermal treatment, 5 mg of the soot sample in platinum crucibles of TGA was performed under a nitrogen atmosphere. The nitrogen environment chosen for thermal treatment is because the nitrogen is approximately 70 % or even more in the exhaust gases passing through a DPF (Reşitoğlu et al., 2014). Moreover, the thermal treatment performed under only a nitrogen environment would isolate the effect of other gas components of exhaust gases on experimental results. Previous studies have demonstrated that thermal treatment at 450 °C for 60 min under an inert gas condition could effectively remove the absorbed unburned hydrocarbons and volatile matters and exert a limited influence on soot properties (Yehliu et al., 2012; Yehliu et al., 2013). Thus, the temperature was heated to 450 °C at first and kept this temperature for 60 min. The diesel soot and carbon black after the removal of these volatile matters were termed DS-D and CB-D. Then the isothermally thermal treatment was carried out under various temperatures for seven hours. The significant thermal deactivation occurs when the thermal treatment temperature is above 500 °C in an inert gas condition (Raj et al., 2014; Gaddam et al., 2016). Consequently, 600 °C, 800 °C, and 1000 °C were chosen as isothermal thermal treatment temperatures to study the variations in soot properties during the thermal deactivation of soot particles. The diesel soot and carbon black after thermal treatment at 600 °C, 800 °C, and 1000 °C are denoted as DS-600, DS-800, DS-1000, CB-600, CB-800, and CB-1000, respectively.

The mass loss of diesel soot and carbon black against the treatment time under various temperatures is shown in Fig.1. There is a slight mass loss for both diesel soot and carbon black at 600 °C. The mass loss for the diesel soot and carbon black all reaches about 9% at 800 °C, while the mass loss at 1000 °C is observed to be up to 28.3 % for diesel soot and 25.6 % for carbon black. Such a mass loss of soot samples is likely to be associated with thermal fragmentation and the decomposition of oxygenated compounds (Chung and Violi, 2011; Wang, 2011; Raj et al., 2014). The occurrence of thermal fragmentation causes the sublimation of small polycyclic aromatic hydrocarbons (PAHs) on the surface of soot samples. On the other hand, the oxygenated compounds existing in soot samples would be desorbed when heated above 500 °C (Song et al., 2006; Raj et al., 2014).

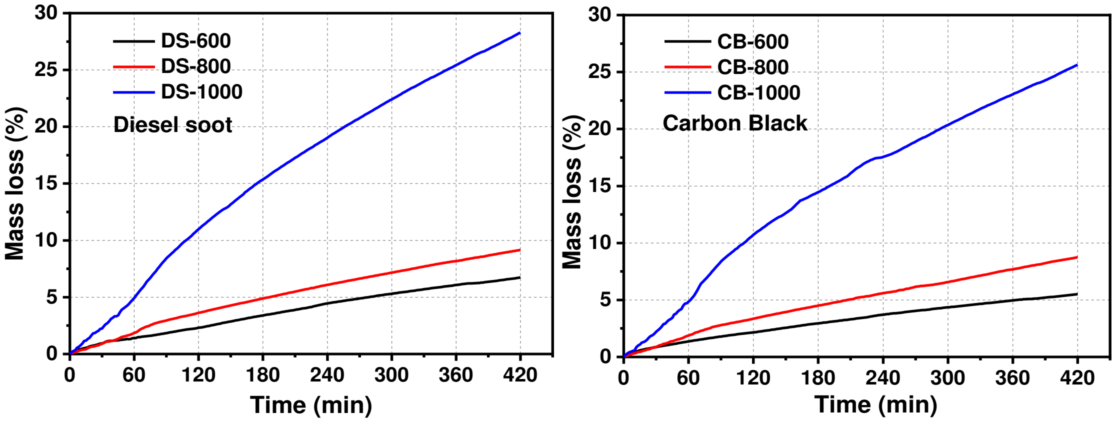

Fig. 1. Mass loss of soot samples during thermal treatment at various temperatures (Liu et al., 2022).

2.3. FT-IR

FT-IR was used to identify and quantify the surface functional groups on the soot surface. FT-IR spectrometer (Nicolet Nexus 470) was employed with a spectral range of 600–3200 cm^{-1} and a resolution of 1 cm^{-1}. The soot samples and analysis grade KBr (0.5 wt%) were mixed and ground, and mixed dispersions were compressed for 5 min at 10 Ton into a thin disk.

2.4. XPS

XPS was implemented to acquire information on the oxygenated functional group and the carbon chemical state in the soot samples. A PerkinElmer PHI-1600 ESCA spectrometer was employed to record XPS spectra using an Mg Kα X-ray source operated at ultra-high vacuum conditions. The C1s peak of contaminant carbon (BE=284.6 eV) was served as an internal standard to calibrate the binding energies. More than three spectra for each sample were obtained to make sure the reproducibility of the tested results.

2.5. RS

Raman spectra were measured by means of Raman microscope system (Renishaw 1000) with and a wavelength of 514.5 nm and an Ar ion excitation laser. Raman spectra in the 900–2000 cm^{-1} range were recorded with an exposure time of 60 s. About 1 mW laser beam power was employed to avoid modifying or burning the soot samples. For each sample, more than three spectra were obtained to make sure the reproducibility of the results.

3. Results and discussion

3.1. Surface functional groups

In the present study, FT-IR was used to identify and quantify the surface functional groups on the soot surfaces. Fig. 2 shows the background-corrected, smoothed FT-IR spectra of diesel soot and carbon black over thermal treatment at various temperatures in the region between 600 and 3200 cm^{-1}. All the soot samples have almost similar positions of peaks but exhibit different signal intensities. Three well-defined aliphatic CH_3 asymmetric stretching, CH_2 asymmetric stretching and CH_3 symmetric stretching peaks are measured at 2960, 2920, and 2850 cm^{-1}, respectively, which are primarily from methylene bridges maintaining the interconnection among PAHs or from methyl, methylene, and methine attached to aromatic rings on PAHs (Ibarra et al., 1996; Santamaria et al., 2006; Liu et al., 2016). The aliphatic C–H plane deformations of CH_2/CH_3 groups are measured and located at 1380 and 1450 cm^{-1}, respectively (Santamaria et al., 2006; Cain et al., 2010). Most of the peaks detected here are also observed for soot particles formed in an inverse diffusion flame (Santamaria et al., 2006; Santamaria et al., 2010). However, no signal of aromatic C–H stretching located at around 3030 cm^{-1} is measured in this study. The aromatic out-of-plane C–H bending vibrations of three-adjacent, two-adjacent and isolated hydrogens are observed at 750, 830, and 880 cm^{-1}, respectively (Santamaria et al., 2006; Russo et al., 2014). The peak at 675 cm^{-1} is measured in this study, which is assigned to aromatic out-of-plane C–H bending vibration (Bladt et al., 2012). In addition, the peaks at 1640 and 1520 cm^{-1} are detected, corresponding to the stretching of alkenyl C=C and aromatic C=C–C groups (Santamaria et al., 2006; Raj et al., 2014). Some oxygen-related functional groups are also measured for the soot samples. The peak of C=O stretching of carboxylic groups is observed at about 1700 cm^{-1} (McKinnon et al., 1996; Kirchner et al., 2000). The oxygen-carbon stretching groups of the ether, esters and hydroxyl appear at 1260, 1100, and 1050 cm^{-1}, respectively (Cain et al., 2010).

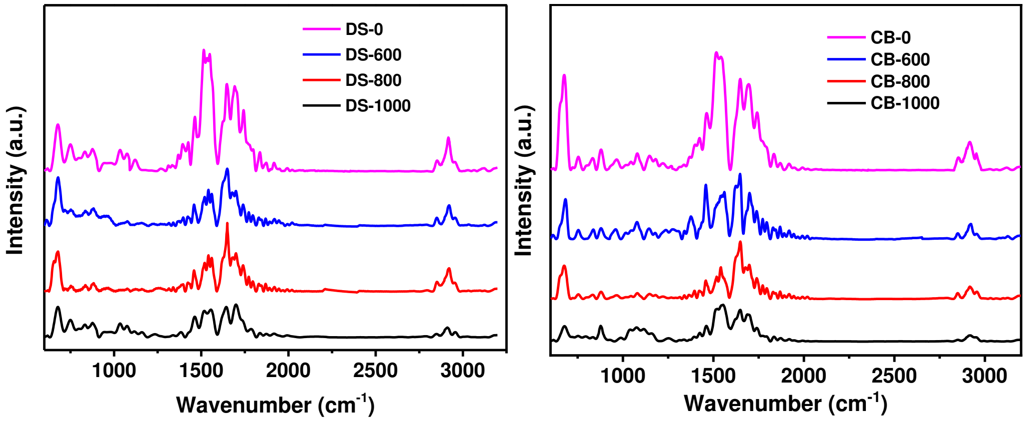

Fig. 2. FT-IR spectra of diesel soot and carbon black over thermal treatment at various temperatures.

3.1.1. Aliphatic and aromatic C–H groups

Given some factors, such as the content and thickness of the KBr pellet, have an impact on the signal intensity in FT-IR spectra, the intensity ratio of the aliphatic C–H peak at 2920 cm^{-1} to the aromatic C=C peak at 1640 cm^{-1} ($I_{\text{Ali}}/I_{\text{C=C}}$) is used to quantify the relative concentration of aliphatic C–H groups in the light of the suggestion by McKinnon et al., (1996) and Santamaría et al., (2007). Fig. 3 presents the variation in the $I_{\text{Ali}}/I_{\text{C=C}}$ ratios as functions of thermal treatment temperatures. The diesel soot and carbon black exhibit the same evolution trend regarding changes in the $I_{\text{Ali}}/I_{\text{C=C}}$ ratios when increasing thermal treatment temperature. The relative content of aliphatic C–H groups reduces gradually with an increase in thermal treatment temperature, indicating that the higher thermal treatment temperature would consume more aliphatic hydrogen. This behavior is primarily ascribed to the following factors: (1) the increased carbonization reactions with increasing thermal treatment temperatures enhance dehydrogenation rates (Wang et al., 2013; Liu et al., 2016); (2) the more cyclic or acyclic aliphatics including aliphatic C–H groups would be desorbed from soot surfaces when heated at higher thermal treatment temperature (Raj et al., 2014). In the study of the soot carbonization process by Vander Wal

(1998), it was found that carbonization reduced the concentration of hydrogen functional groups. Dobbins et al., (1995, 1996) stated that the carbonization reaction would reduce aliphatic C–H functional groups on soot surfaces.

Aliphatic C–H groups are a crucial factor affecting soot oxidation reactivity (Wang et al., 2013). The abstraction of H-atoms in aliphatic C–H groups requires lower energy, and the preferential loss of aliphatic hydrogen enhances the number of active sites, increasing soot reactivity (Santamaria et al., 2006). As a result, the concentration of aliphatic C–H functional groups reduces when increasing thermal treatment temperature, which decreases the number of actives sites and lowers soot reactivity. Agudelo et al., (2014) investigated the soot particles from diesel and crude vegetable oils. The results presented that the reduction in aliphatic C–H groups led to the decreased reactivity. The same conclusion was reached by Ruiz et al., (2015), who found that the soot reactivity reduced as the concentration of aliphatic C–H groups decreased. Soriano et al., (2017) discovered that soot generated from paraffinic fuel had higher reactivity than that from diesel fuel. They revealed that this higher reactivity was due to a higher concentration of aliphatic functional groups.

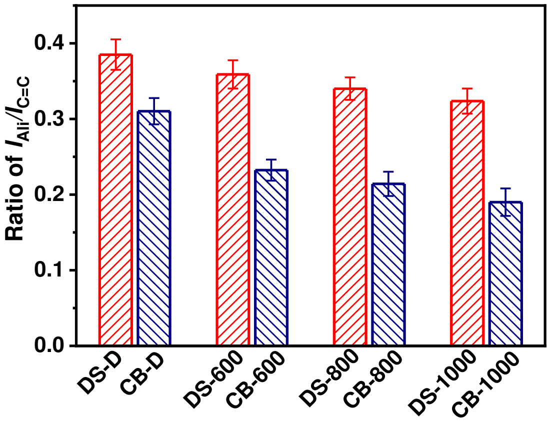

Fig. 3. Relative concentrations of aliphatic C–H functional groups as functions of thermal treatment temperature.

3.1.2. Oxygenated functional groups

XPS analyses in this study were carried out to gain information regarding the oxygenated functional groups and carbon chemical state. Fig. 4 presents a representative high-resolution scan of the C1s peak. The C1s region was deconvoluted to four peaks according to the method suggested in the literature (Pumera and Iwai, 2009; Gaddam and Vander Wal, 2013): the peak at 286.6 eV assigned to hydroxyl (C–OH) groups, the peak at 288.4 eV corresponding to carbonyl (C=O) group, and the peak at 289.2 eV referring to the carboxylic acid (O–C=O) group. The analysis of sp^2 and sp^3 hybridized carbons will be discussed in detail in the subsequent section. The concentrations of C–OH, O–C=O and C=O groups for diesel soot and carbon black are plotted against thermal treatment temperatures in Fig. 5. The contents of C–OH, O–C=O and C=O groups reduce when increasing the thermal treatment temperature, indicating that the more oxygenated functional groups are desorbed at the higher temperature. According to previous work (Song et al., 2007; Lapuerta et al., 2020), the oxygenated groups are important intermediate compounds and exert a crucial influence on oxidation reaction, influencing soot reactivity. In the present work, the oxygenated functional groups for soot samples decrease with the increase in thermal treatment temperature, which in turn reduced soot reactivity. Song et al., (2006) probed the correlation between the oxygenated functional groups and reactivity and found that the decreased relative concentration of oxygenated functional groups would reduce soot reactivity. Soriano et al., (2017) came to the same conclusion, and the results revealed that the biodiesel soot possessed higher concentrations of oxygenated functional groups compared to diesel soot and had higher oxidative reactivity. However, a different conclusion was obtained by Yehliu et al., (2012), who found that the content of oxygenated functional groups was not associated with soot reactivity.

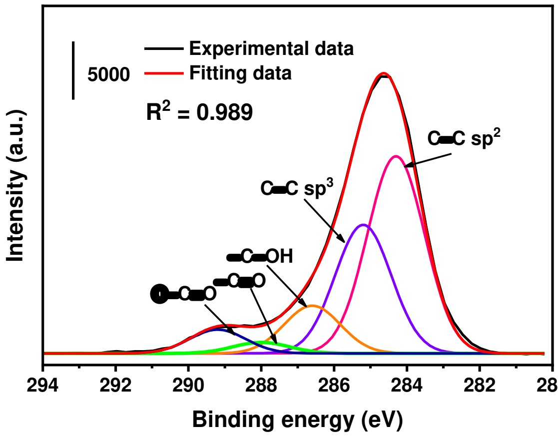

Fig. 4. Representative XPS C 1s narrow spectra for DS-D

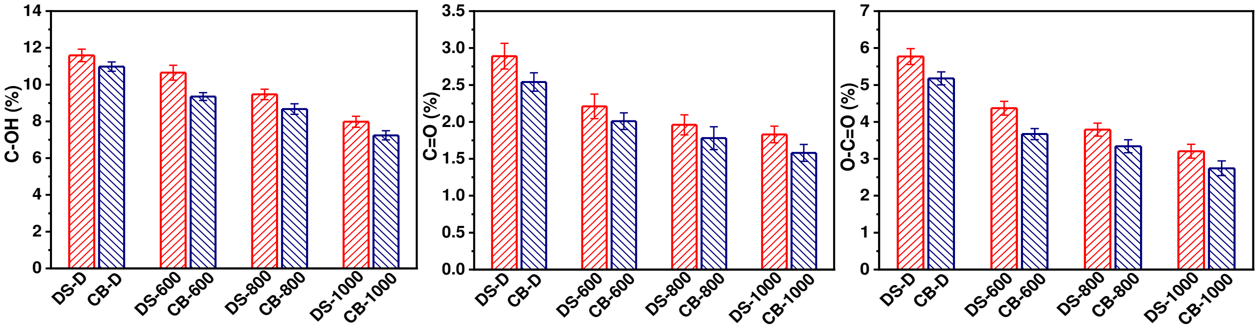

Fig. 5. Contents of C–OH, O–C=O and C=O groups as functions of thermal treatment temperature.

The percentage reductions of C–OH, C=O and O–C=O groups for diesel soot and carbon black are calculated with various thermal treatment temperatures. Compared to DS-D, the concentrations of C–OH, C=O and O–C=O groups for DS-1000 reduce by 31%, 37%, and 44%. Similarly, the contents of C–OH, C=O and O–C=O groups for CB-1000 decrease by 34%, 38% and 47% than those for CB-D. The percentage reduction for diesel soot and carbon black follows the sequence: O–C=O > C=O > C–OH groups, which is likely to be correlated with the relative thermodynamic stability of these oxygenated functional groups. In the study by Vander Wal et al., (2010), it was discovered that the relative thermodynamic stability of C–OH, C=O and O–C=O groups decreases sequentially. As a result, the O–C=O groups have the worst thermodynamic stability, and thus the percentage reduction is the largest for the O–C=O groups.

3.2. Carbon chemical state

XPS was also used to gain chemical information regarding the sp^2 and sp^3 hybridized carbon atoms (Tandon and Rosner, 1996; Vander Wal et al., 2014). The sp^2 and sp^3 hybridized carbon atoms are integral to the overall soot nanostructure. As shown in Fig. 4, the deconvolution of the high-resolution spectrum about the C1s region was performed to quantify the relative contents of sp^2 and sp^3 hybridized carbon atoms. The peak near 284.3 eV is a representation of sp^2 hybridized carbons and π bonding in soot (Raj et al., 2014; Guerrero Peña et al., 2016). The peak near 285.2 eV is assigned to the sp^3 hybridized carbons and σ bonding in soot (Raj et al., 2014; Guerrero Peña et al., 2016). The sp^2 hybridized carbons refer to the ordered carbon, and the sp^3 hybridized carbon atoms would affect the sp^2 hybridized network and need bond terminations other than adjacent π bonded carbon atoms. These sp^3 hybridized carbon atoms would reduce the structural order and are consequently considered as the defect sites (Vander Wal et al., 2011). Thus, a large sp^2/sp^3 hybridization ratio corresponds to a more ordered structure (Alfe et al., 2009).

Fig. 6 shows the sp^2/sp^3 values for diesel soot and carbon black as functions of thermal treatment temperature. Compared to diesel soot, carbon black has slightly larger sp^2/sp^3 values at each thermal treatment temperature. In addition, a monotonic increase trend in sp^2/sp^3 hybridization ratios for diesel soot and carbon black is observed with increasing thermal treatment temperature, demonstrating that soot samples transform towards a more ordered structure as thermal treatment temperature increases. This behavior is primarily due to the desorption of more amorphous species on soot surfaces when increasing thermal treatment temperature. Raj et al., (2014) also reported that amorphous and disorder species were desorbed from soot surfaces, which included a large quantity of cyclic or acyclic aliphatics. In the study by Fetzer (2000), it was found that some amorphous PAHs making up soot particles would be sublimated at approximately 500 °C. Consequently, more amorphous PHAs will be sublimated when heated above 500 °C, which favours soot samples towards a better graphitic organization, corresponding to the increased sp^2/sp^3 ratio. In addition, it was found through a theoretical calculation that the binding energy of the PAHs on soot surfaces was closely related to the mass of PAHs in the stack, and small PAHs had lower binding energy relative to the large ones (Herdman and Miller, 2008; Raj et al., 2011). As a result, there is a high probability for amorphous and small PAHs that can escape from the PAHs stacks in soot by overcoming van der Waals force of attraction, which develops a more ordered structure, in line with the current XPS data. An increase in sp^2/sp^3 hybridization ratio corresponds to an enhancement in graphitic planar structures within soot samples, which reduces active sites for oxygen attack and thus lowers soot reactivity (Alfe et al., 2009). A similar finding was reported by Gaddam et al., (2016), who pointed out that the large sp^2/sp^3 hybridization ratio for the model carbon presented low reactivity. Fan et al., (2019) revealed that the diesel soot particles with the large sp^2/sp^3 hybridization ratio presented more resistance to oxidation.

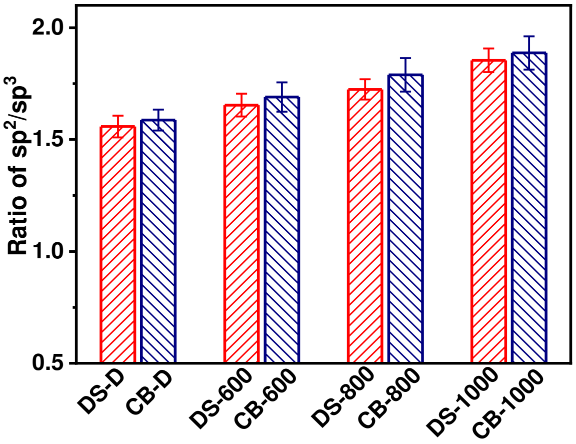

Fig. 6. Sp^2/sp^3 hybridization ratios as functions of thermal treatment temperature.

3.3. Graphitization degree

RS was employed to assess the graphitization degree of the soot samples. Fig. 7 shows the representative baseline-corrected, smoothed spectra of DS-1000 and CB-1000. It can be observed that these two spectra show two broad peaks at around 1350 cm^{-1} (D peak) and 1600 cm^{-1} (G peak). For quantitative analysis, the spectrum of each soot sample is deconvoluted and fitted by three Lorentian functions and one Gaussian function (Seong and Boehman, 2013), as shown in Fig. 8. The Lorentzian functions refer to the D1 band assigned to the carbon atoms at the edge sites of the graphene layers (Seong and Boehman, 2011), the D4 band arising from the C=C and C–C bands (Cuesta et al., 1994; Dippel et al., 1999), and the G band as a result of the ideal graphitic lattice (Seong and Boehman, 2013; Ge et al., 2019), while the Gaussian function corresponds to the D3 band arising from the amorphous carbon of the soot (Cuesta et al., 1994; Parent et al., 2016).

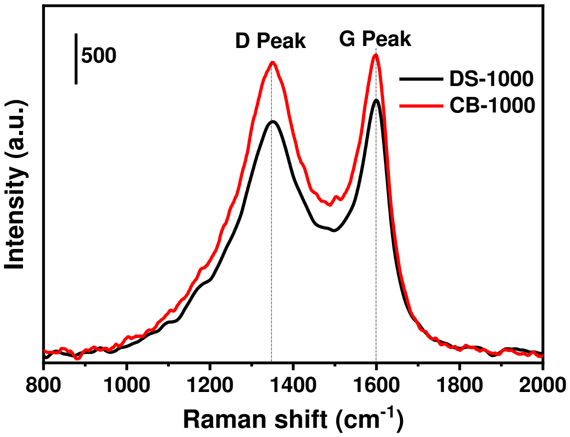

Fig. 7. Representative Raman spectra of DS-1000 and CB-1000.

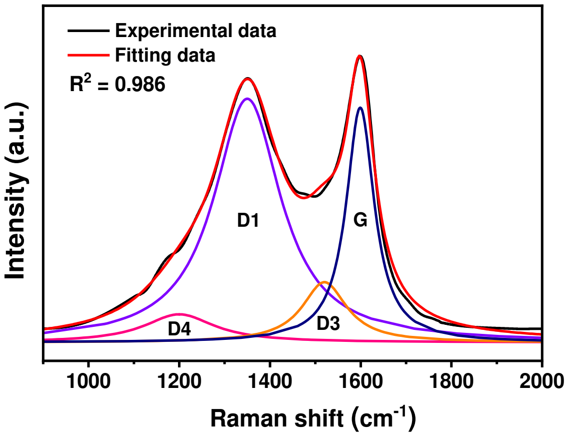

Fig. 8. Four-band fitting of representative Raman spectrum for DS-1000.

The peak intensity ratios of the D1 band or the full width at half maximum (FWHM) of the bands to the G band were frequently employed to determine the graphitization degree of carbon materials (Yoshida et al., 2006; Sheng, 2007; Zaida et al., 2007). However, only the peak intensity ratio or the FWHM of the bands is likely unable to be a complete representation of the evolution of soot structural order. By contrast, the peak area ratio (integrated intensity) is the function of the FWHM and the peak intensity, which includes the effect of these two parameters. As a result, the peak area ratios of D1 to G (A_{D1}/A_G) are used to evaluate the graphitization degree of soot samples in the present study. A lower A_{D1}/A_G ratio indicates a more ordered structure in soot (Tuinstra and Koenig, 1970; Sheng, 2007). Fig. 9 shows the change in graphitization degree of soot samples against various thermal treatment temperatures. Compared to diesel soot, the carbon black is observed to have a lower value of A_{D1}/A_G ratio at the same thermal treatment temperature. For the diesel soot and carbon black, the values of A_{D1}/A_G reduce from 1.89 to 1.59 and from 1.85 to 1.56 with the temperature increasing from 600 to 1000 °C, respectively, indicating the transformation towards more-ordered structure for both soot samples. Such a structural transformation is mainly because the amorphous species on the soot surfaces are desorbed during thermal treatment (Sheng, 2007; Zaida et al., 2007; Raj et al., 2014). Compared to carbon atoms in the basal plane, the carbon atoms at the edge sites of the graphene were reported to have 100-1000 times more reactive (Marsh and Kuo, 1989; Vander Wal and Tomasek, 2004; Vander Wal and Mueller, 2006). The thermally treated soot samples possess more ordering of the soot crystallite structure, corresponding to the lower ratio of edge to base carbon atoms. As a result, soot samples after thermal treatment present more resistance towards oxidation. A similar finding was reported by Sheng (2007), who studied the structure and reactivity of coal chars under different thermal treatment conditions and identified that the thermal deactivation of coal char was dependent on the structural ordering of char crystallite. Feng et al., (2002) probed the change in the structural ordering of coal char during thermal treatment and the effect on its reactivity. The results revealed that the decrease in reactivity during thermal treatment was due to a crystallite-perfecting process. Raj et al., (2014) believed that thermal treatment decreased the number of carbon atoms at the edge sites for reaction, thus lowering soot reactivity.

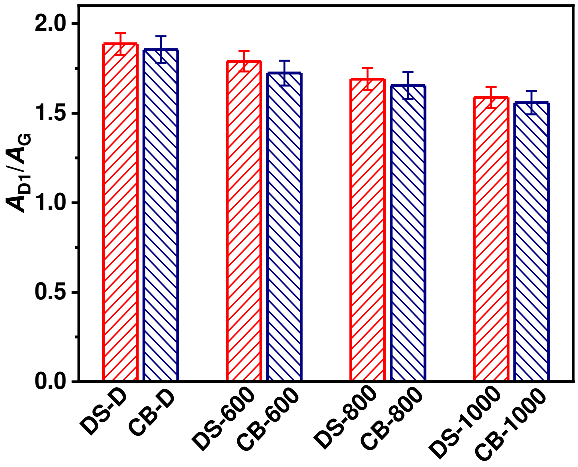

Fig. 9. A_{D1}/A_G ratios as functions of thermal treatment temperature.

Close observation of Figs. 3, 5, 6, and 9 present that considering the uncertainties of aliphatic C−H groups, oxygenated functional groups, sp^2/sp^3 ratio, and A_{D1}/A_G ratio, it appears to be no significant difference in the average values among these properties of thermally treated samples. To determine the statistical differences, the statistical analysis, one-way analysis of variance (ANOVA), was conducted. For all results, the p values obtained from the statistical analysis are lower than 0.05, suggesting that such differences are statistically significant. It worth mentioning that the Printex-U in the previous studies was frequently employed as a surrogate for diesel soot (Vander Wal et al., 2007; Arnal et al., 2012). However, our current results show that the aliphatic C−H groups, oxygenated functional groups, carbon chemical state and graphitization degree for diesel soot are statistically different from those for the Printex-U, which is likely due to a lower proportion in heteroatoms and a higher graphitic order for the Printex-U (Jaramillo et al., 2015). Additionally, soot properties emitted from a diesel engine are affected significantly by diesel engine type, engine speed and engine load (Lapuerta et al., 2020). As a result, whether the Printex-U can be employed as the best surrogate for diesel soot to perform related research remains to be further studied.

4. Conclusions

Variations in surface functional groups, carbon chemical state and graphitization degree of diesel soot and a commercial carbon black was studied during thermal deactivation. The mass loss of diesel soot and carbon black increases with increasing the thermal treatment temperature, particularly at 1000 °C, around 29 % mass loss can be observed for diesel soot. The concentrations of aliphatic C–H groups, C–OH, C=O, and O–C=O groups reduce for diesel soot and carbon black when increasing thermal treatment temperature, whereas the sp^2/sp^3 hybridized ratio and graphitization degree enhance. These results can provide further evidence for thermal deactivation during thermal treatment. Compared to diesel soot, the commercial carbon black has lower concentrations of aliphatic C–H groups, C–OH, C=O and O–C=O groups and higher graphitization degree and sp^2/sp^3 hybridized ratio at the same thermal treatment temperature. Among oxygenated functional groups, the percentage reduction during thermal treatment is largest for the O–C=O groups due to its worst thermodynamic stability.

5. Acknowledgments

This research is supported by the National Natural Science Foundation of China (No. 52006054), the State Key Laboratory of Engines at Tianjin University (Grant No. K2021-05) and the European Union’s project MODALES (grant agreement No. 815189).

6. References

Agudelo, J.R., Álvarez, A., Armas, O., 2014. Impact of crude vegetable oils on the oxidation reactivity and nanostructure of diesel particulate matter. Combustion and Flame 161, 2904-2915.

Alfè, M., Apicella, B., Barbella, R., Rouzaud, J.N., Tregrossi, A., Ciajolo, A., 2009. Structure–property relationship in nanostructures of young and mature soot in premixed flames. Proceedings of the Combustion Institute 32, 697-704.

Arnal, C., Alzueta, M.U., Millera, A., Bilbao, R., 2012. Influence of water vapor addition on soot oxidation at high temperature. Energy 43, 55-63.

Bladt, H., Schmid, J., Kireeva, E.D., Popovicheva, O.B., Perseantseva, N.M., Timofeev, M.A., Heister, K., Uihlein, J., Ivleva, N.P., Niessner, R., 2012. Impact of Fe Content in Laboratory-Produced Soot Aerosol on its Composition, Structure, and Thermo-Chemical Properties. Aerosol Science and Technology 46, 1337-1348.

Cain, J.P., Gassman, P.L., Wang, H., Laskin, A., 2010. Micro-FTIR study of soot chemical composition—evidence of aliphatic hydrocarbons on nascent soot surfaces. Physical Chemistry Chemical Physics 12, 5206.

Chung, S.-H., Violi, A., 2011. Peri-condensed aromatics with aliphatic chains as key intermediates for the nucleation of aromatic hydrocarbons. Proceedings of the Combustion Institute 33, 693-700.

Cuesta, A., Dhamelincourt, P., Laureyns, J., Martínez-Alonso, A., Tascón, J.M.D., 1994. Raman microprobe studies on carbon materials. Carbon 32, 1523-1532.

Dippel, B., Janderb, H., Heintzenberga, J., 1999. NIR FT Raman spectroscopic study of flame soot. Physical Chemistry Chemical Physics 1, 4707-4712.

Dobbins, R.A., Fletcher, R.A., Lu, W., 1995. Laser microprobe analysis of soot precursor particles and carbonaceous soot. Combustion and Flame 100, 301-309.

Dobbins, R.A., Govatzidakis, G.J., Lu, W., Schwartzman, A.F., Fletcher, R.A., 1996. Carbonization Rate of Soot Precursor Particles. Combustion Science and Technology 121, 103-121.

Fan, C., Song, C., Lv, G., Wei, J., Zhang, X., Qiao, Y., Liu, Y., 2019. Impact of post-injection strategy on the physicochemical properties and reactivity of diesel in-cylinder soot. Proceedings of the Combustion Institute 37, 4821-4829.

Feng, B., Bhatia, S.K., Barry, J.C., 2002. Structural ordering of coal char during heat treatment and its impact on reactivity. Carbon 40, 481-496.

Fetzer, J.C., 2000. Large (C= 24) polycyclic aromatic hydrocarbons: chemistry and analysis. John Wiley & Sons, .

Gaddam, C.K., Vander Wal, R.L., 2013. Physical and chemical characterization of SIDI engine particulates. Combustion and Flame 160, 2517-2528.

Gaddam, C.K., Vander Wal, R.L., Chen, X., Yezerets, A., Kamasamudram, K., 2016. Reconciliation of carbon oxidation rates and activation energies based on changing nanostructure. Carbon 98, 545-556.

Ge, H., Ye, Z., He, R., 2019. Raman spectroscopy of diesel and gasoline engine-out soot using different laser power. Journal of Environmental Sciences 79, 74-80.

Guerrero Peña, G.D.J., Alrefaai, M.M., Yang, S.Y., Raj, A., Brito, J.L., Stephen, S., Anjana, T., Pillai, V., Al Shoaibi, A., Chung, S.H., 2016. Effects of methyl group on aromatic hydrocarbons on the nanostructures and oxidative reactivity of combustion-generated soot. Combustion and Flame 172, 1-12.

Herdman, J.D., Miller, J.H., 2008. Intermolecular potential calculations for polynuclear aromatic hydrocarbon clusters. The Journal of Physical Chemistry A 112, 6249-6256.

Ibarra, J., Muñoz, E., Moliner, R., 1996. FTIR study of the evolution of coal structure during the coalification process. Organic Geochemistry 24, 725-735.

Jaramillo, I.C., Gaddam, C.K., Vander Wal, R.L., Lighty, J.S., 2015. Effect of nanostructure, oxidative pressure and extent of oxidation on model carbon reactivity. Combustion and Flame 162, 1848-1856.

Kirchner, U., Scheer, V., Vogt, R., 2000. FTIR Spectroscopic Investigation of the Mechanism and Kinetics of the Heterogeneous Reactions of NO2 and HNO3 with Soot. The Journal of Physical Chemistry A 104, 8908-8915.

Lapuerta, M., Rodríguez–Fernández, J., Sánchez-Valdepeñas, J., 2020. Soot reactivity analysis and implications on diesel filter regeneration. Progress in Energy and Combustion Science 78.

Liu, Y., Fan, C., Wang, X., Liu, F., Chen, H., 2022. Thermally induced variations in the nanostructure and reactivity of soot particles emitted from a diesel engine. Chemosphere 286, 131712.

Liu, Y., Song, C., Lv, G., Cao, X., Wang, L., Qiao, Y., Yang, X., 2016. Surface functional groups and sp 3 /sp 2 hybridization ratios of in-cylinder soot from a diesel engine fueled with n -heptane and n -heptane/toluene. Fuel 179, 108-113.

Liu, Y., Song, C., Lv, G., Wang, X., Li, N., 2017. Virgin and Extracted Soots in Premixed Methane Flames: A Comparison of Surface Functional Groups, Graphitization Degree, and Oxidation Reactivity. Energy & Fuels 31, 6413-6421.

Marsh, H., Kuo, K., 1989. Kinetics and catalysis of carbon gasification. Introduction to carbon science. Elsevier, pp. 107-151.

Matsumoto, K., Tojo, M., Jinnai, Y., Hayashi, N., Ibaraki, S., 2008. Development of compact and high-performance turbocharger for 1,050 C exhaust gas. Mitsubishi Heavy Industries Technical Review 45.

McKinnon, J.T., Meyer, E., Howard, J.B., 1996. Infrared analysis of flame-generated PAH samples. Combustion and Flame 105, 161-166.

Parent, P., Laffon, C., Marhaba, I., Ferry, D., Regier, T.Z., Ortega, I.K., Chazallon, B., Carpentier, Y., Focsa, C., 2016. Nanoscale characterization of aircraft soot: A high-resolution transmission electron microscopy, Raman spectroscopy, X-ray photoelectron and near-edge X-ray absorption spectroscopy study. Carbon 101, 86-100.

Pumera, M., Iwai, H., 2009. Multicomponent metallic impurities and their influence upon the electrochemistry of carbon nanotubes. The Journal of Physical Chemistry C 113, 4401-4405.

Raj, A., Tayouo, R., Cha, D., Li, L., Ismail, M.A., Chung, S.H., 2014. Thermal fragmentation and deactivation of combustion-generated soot particles. Combustion and Flame 161, 2446-2457.

Raj, A., Yang, S.Y., Cha, D., Tayouo, R., Chung, S.H., 2013. Structural effects on the oxidation of soot particles by O2: Experimental and theoretical study. Combustion and Flame 160, 1812-1826.

Raj, A., Zainuddin, Z., Sander, M., Kraft, M., 2011. A mechanistic study on the simultaneous elimination of soot and nitric oxide from engine exhaust. Carbon 49, 1516-1531.

Reşitoğlu, I.A., Altinişik, K., Keskin, A., 2014. The pollutant emissions from diesel-engine vehicles and exhaust aftertreatment systems. Clean Technologies and Environmental Policy 17, 15-27.

Roth, P., Eckhardt, T., Franz, B., Patschull, J., 1998. H2O2-assisted regeneration of diesel particulate traps at typical exhaust gas temperatures. Combustion and Flame 115, 28-37.

Ruiz, F.A., Cadrazco, M., López, A.F., Sanchez-Valdepeñas, J., Agudelo, J.R., 2015. Impact of dual-fuel combustion with n-butanol or hydrous ethanol on the oxidation reactivity and nanostructure of diesel particulate matter. Fuel 161, 18-25.

Russo, C., Stanzione, F., Tregrossi, A., Ciajolo, A., 2014. Infrared spectroscopy of some carbon-based materials relevant in combustion: Qualitative and quantitative analysis of hydrogen. Carbon 74, 127-138.

Santamaria, A., Mondragon, F., Molina, A., Marsh, N., Eddings, E., Sarofim, A., 2006. FT-IR and 1H NMR characterization of the products of an ethylene inverse diffusion flame. Combustion and Flame 146, 52-62.

Santamaría, A., Mondragón, F., Quiñónez, W., Eddings, E.G., Sarofim, A.F., 2007. Average structural analysis of the extractable material of young soot gathered in an ethylene inverse diffusion flame. Fuel 86, 1908-1917.

Santamaria, A., Yang, N., Eddings, E., Mondragon, F., 2010. Chemical and morphological characterization of soot and soot precursors generated in an inverse diffusion flame with aromatic and aliphatic fuels. Combustion and Flame 157, 33-42.

Schejbal, M., Marek, M., Kubíček, M., Kočí, P., 2009. Modelling of diesel filters for particulates removal. Chemical Engineering Journal 154, 219-230.

Seong, H.J., Boehman, A.L., 2011. Impact of Intake Oxygen Enrichment on Oxidative Reactivity and Properties of Diesel Soot. Energy & Fuels 25, 602-616.

Seong, H.J., Boehman, A.L., 2013. Evaluation of Raman Parameters Using Visible Raman Microscopy for Soot Oxidative Reactivity. Energy & Fuels 27, 1613-1624.

Sheng, C., 2007. Char structure characterised by Raman spectroscopy and its correlations with combustion reactivity. Fuel 86, 2316-2324.

Song, J., Alam, M., Boehman, A.L., 2007. Impact of alternative fuels on soot properties and DPF regeneration. Combustion Science and Technology 179, 1991-2037.

Song, J., Alam, M., Boehman, A.L., Kim, U., 2006. Examination of the oxidation behavior of biodiesel soot. Combustion and Flame 146, 589-604.

Soriano, J.A., Agudelo, J.R., López, A.F., Armas, O., 2017. Oxidation reactivity and nanostructural characterization of the soot coming from farnesane-A novel diesel fuel derived from sugar cane. Carbon 125, 516-529.

Tandon, P., Rosner, D.E., 1996. Sintering kinetics and transport property evolution of large multi-particle aggregates. Chemical Engineering Communications 151, 147-168.

Tuinstra, F., Koenig, J.L., 1970. Raman spectrum of graphite. The Journal of chemical physics 53, 1126-1130.

Vander Wal, R.L., 1998. Soot precursor carbonization: Visualization using LIF and LII and comparison using bright and dark field TEM. Combustion and Flame 112, 607-616.

Vander Wal, R.L., Bryg, V.M., Hays, M.D., 2010. Fingerprinting soot (towards source identification): Physical structure and chemical composition. Journal of Aerosol Science 41, 108-117.

Vander Wal, R.L., Bryg, V.M., Hays, M.D., 2011. XPS analysis of combustion aerosols for chemical composition, surface chemistry, and carbon chemical state. Analytical Chemistry 83, 1924-1930.

Vander Wal, R.L., Bryg, V.M., Huang, C.-H., 2014. Aircraft engine particulate matter: Macro- micro- and nanostructure by HRTEM and chemistry by XPS. Combustion and Flame 161, 602-611.

Vander Wal, R.L., Bryg, V.M., Huang, C.-H., 2016. Chemistry characterization of jet aircraft engine particulate matter by XPS: Results from APEX III. Atmospheric Environment 140, 623-629.

Vander Wal, R.L., Mueller, C.J., 2006. Initial Investigation of Effects of Fuel Oxygenation on Nanostructure of Soot from a Direct-Injection Diesel Engine. Energy & Fuels 20, 2364-2369.

Vander Wal, R.L., Tomasek, A.J., 2004. Soot nanostructure: dependence upon synthesis conditions. Combustion and Flame 136, 129-140.

Vander Wal, R.L., Tomasek, A.J., Street, K., Hull, D.R., Thompson, W.K., 2004. Carbon nanostructure examined by lattice fringe analysis of high-resolution transmission electron microscopy images. Applied Spectroscopy 58, 230-237.

Vander Wal, R.L., Yezerets, A., Currier, N.W., Kim, D.H., Wang, C.M., 2007. HRTEM Study of diesel soot collected from diesel particulate filters. Carbon 45, 70-77.

Wang, H., 2011. Formation of nascent soot and other condensed-phase materials in flames. Proceedings of the Combustion Institute 33, 41-67.

Wang, L., Song, C., Song, J., Lv, G., Pang, H., Zhang, W., 2013. Aliphatic C–H and oxygenated surface functional groups of diesel in-cylinder soot: Characterizations and impact on soot oxidation behavior. Proceedings of the Combustion Institute 34, 3099-3106.

Xu, L., Lingaswamy, A.P., Zhang, Y., Liu, L., Wang, Y., Zhang, J., Ma, Q., Li, W., 2019. Morphology, composition, and sources of individual aerosol particles at a regional background site of the YRD, China. Journal of Environmental Sciences 77, 354-362.

Yehliu, K., Armas, O., Vander Wal, R.L., Boehman, A.L., 2013. Impact of engine operating modes and combustion phasing on the reactivity of diesel soot. Combustion and Flame 160, 682-691.

Yehliu, K., Vander Wal, R.L., Armas, O., Boehman, A.L., 2012. Impact of fuel formulation on the nanostructure and reactivity of diesel soot. Combustion and Flame 159, 3597-3606.

Yoshida, A., Kaburagi, Y., Hishiyama, Y., 2006. Full width at half maximum intensity of the G band in the first order Raman spectrum of carbon material as a parameter for graphitization. Carbon 44, 2333-2335.

Zaida, A., Bar-Ziv, E., Radovic, L.R., Lee, Y.-J., 2007. Further development of Raman microprobe spectroscopy for characterization of char reactivity. Proceedings of the combustion institute 31, 1881-1887.

Zhou, Q., Wang, Y., Wang, X., Bai, Y., 2022. Experimental investigation into the oxidation reactivity, morphology and graphitization of soot particles from diesel/n-octanol mixtures. Journal of Environmental Sciences 112, 218-230.

Zolin, A., Jensen, A.D., Jensen, P.A., Dam-Johansen, K., 2002. Experimental study of char thermal deactivation. Fuel 81, 1065-1075.